J. Phys. G: Nucl. Part. Phys. 20 (1994) 1243–1256. Printed in the UK

Pocket and barrier resonances in potential scattering and their application to heavy-ion reactions

P Susan, B Sahu, B M Jyrwa and C S Shastry
Department of Physics, North Eastern Hill University, Shillong-793003, Meghalaya, India

Received 12 July 1993, in final form 8 December 1993

Abstract. A comparative study of the properties of pocket and barrier resonances is carried out using finite-range potentials having a pocket and a barrier. Comparison is made between the *s*-wave potential barrier region resonances with an absorptive pocket, and the corresponding resonances of a potential barrier without an absorptive pocket. We numerically study the resonance states generated by the finite-range truncated parabolic barrier. In this case the location of resonances in the vicinity of the barrier are approximately equispaced, but deviation from this feature occurs for resonances farther away from the barrier top. Using these results as a basis we empirically analyse the resonances in the $^{16}O + ^{16}O$ system within the broad framework of the barrier region resonance model.

1. Introduction

The resonance phenomenon generated by the interaction between colliding systems and its role in the analysis of the scattering cross-section is an important aspect of scattering theory. In the S-matrix analysis, bound states and resonance states are analysed in a unified way in terms of the poles of the S-matrix in the complex momentum or energy plane [1, 2]. The S-matrix $S_l(k)$ treated as the complex function $S_l(k) = S_\lambda(k)$ where $\lambda = l + \frac{1}{2}$ is generally analysed in terms of the Jost functions $f_\lambda(k)$ and $f_\lambda(-k)$ [1], i.e.

$$S_\lambda(k) = e^{i\pi(\lambda - 1/2)} f_\lambda(k)/f_\lambda(-k). \tag{1}$$

The poles of the S-matrix are searched in terms of the zeros of the Jost function $f_\lambda(-k)$. The poles of the S-matrix occurring on the positive imaginary axis in the complex momentum (k) plane are associated with bound states, whereas the poles corresponding to

$$k = k_R = \mathrm{Re}\, k_R - i\, \mathrm{Im}\, k_R \tag{2}$$

occurring in the lower half of the complex k plane can be identified as resonances, if $\mathrm{Im}\, k_R$ is less than $\mathrm{Re}\, k_R$. This is because the resonance poles represent decaying states with positive energy

$$E_R = (\mathrm{Re}\, k_R)^2 - (\mathrm{Im}\, k_R)^2 \tag{3}$$

and finite width

$$\Gamma = 4\, \mathrm{Re}\, k_R\, \mathrm{Im}\, k_R. \tag{4}$$

0954-3899/94/081243 + 14$19.50

The smaller the $\mathrm{Im}\, k_R$ the narrower is the width, and hence it corresponds to a long-lived resonance.

Such a formal analysis of the S-matrix does not readily help us in identifying the physical origin of resonances and their localization in the configuration space of two colliding systems. However, this can be achieved from the strength and shape of the potential generating these structures. It is found that in potential scattering, the potential pocket, barrier and absorption have important roles in determining the nature of resonances. In the past few years interesting work has been done in this area [3, 4], and hence further investigation in this line is desirable, since it will help us in constructing appropriate models for explaining resonances in heavy-ion reactions.

In the case of a finite-range potential with a pocket followed by a barrier we can identify two important possibilities:

(i) The resonances occurring below the barrier and the wavefunctions corresponding to which are localized predominantly in the pocket, can be termed pocket resonances (PRS). These resonance states can decay by tunnelling away from the pocket across the barrier to infinity. If the effective barrier for a given state is large, the decay probability will be small, and as a consequence, sharp resonances will be generated.

(ii) If the resonance energies are on the top of the barrier and the wavefunctions are dominant in the barrier region, they can be termed finite-range barrier resonances (FRBRS). In fact, one can visualize such resonances as a result of a slowing down of the relative radial velocity of the colliding system in the barrier region.

In a collision process the colliding system sees an effective potential for each partial wave which is the sum of the scattering potential and the centrifugal term. The latter introduces a very large repulsion near the origin. In the case of a potential with a pocket followed by a barrier the centrifugal term systematically varies the effective potential as a function of l, making the potential pocket shallower and shallower and slowly increasing the barrier height as l increases. Such a situation occurs in the case of real potentials between two heavy-ion systems. One of the objectives of the present paper is to clearly distinguish the nature and properties of PRS and FRBRS occurring in finite-range potentials. We also study the consequence of a large absorption in the pocket region using relevant examples. Since a typical nucleus–nucleus potential has a pocket and a barrier with large absorption in the pocket, this analysis can be extended to explain the resonances in heavy-ion reactions. As an illustration of the above approach we study the resonances in a typical heavy-ion collision system, namely $^{16}O + {}^{16}O$, in terms of FRBRS.

The pioneering work on what are defined as barrier top resonances (BTRS) has been done by Friedman and Goebel [5] using the Hamiltonian for the inverted parabolic barrier

$$H = -\frac{\delta x^2}{2m} + V_0 - \frac{m\nu^2 x^2}{2} \tag{5}$$

and they showed that the corresponding resonance states have the energy

$$E_n = V_0 - \mathrm{i}(n + \tfrac{1}{2})\nu. \tag{6}$$

They have also generalized this in the case of scattering in three dimensions, for which the resonance poles are at

$$E_{n_r,l} = V_0 - \mathrm{i}(2n_r + l + \tfrac{3}{2})\nu. \tag{7}$$

These resonances are of a special type in the sense that all of them have the same energy corresponding to the barrier top V_0 and steadily increasing widths. In the same paper [5] they indicate that in the case of a barrier of height V_B located at $r = R_B$ their model of BTRS based on an inverted barrier is appropriate for the study of resonances when there is infinite absorption introduced to the left of the barrier. They have also discussed the application of such a model to heavy-ion reactions.

The definition of BTRS as given in (7) indicates that at a given energy $E = V_0$ and for a given l, corresponding to the barrier top, there is a large number of superposing resonances with increasing width. On the other hand, in observed heavy-ion resonances we expect a set of discrete resonances for any given l. In this connection it may be noted that the definition of BTRS as given in [5] corresponds to an infinite-range barrier, and the corresponding situation can be expected to be somewhat different in the case of a more realistic finite-range potential with the pocket and the barrier. That is to say that the definition corresponding to (7) pertains to resonances generated by a special type of barrier whereas in more realistic situations the resonances can be expected to occur as a result of an interplay between the barrier and the pocket together with absorption. In situations where the pocket is highly absorptive, the barrier region resonances can be expected to be important. Such a situation can occur in nucleus–nucleus collisions. Hence in the present paper we distinguish the resonances in the barrier region from BTRS as defined in [5] by using the term 'FRBRS'.

This paper is organized in the following way. In section 2 we carry out a comparative study of the properties of PRS and FRBRS using some model calculations. In section 3 we describe the barrier region resonance model for the $^{16}O + {}^{16}O$ system using the resonances generated by a truncated parabolic barrier. Finally in section 4 we present a discussion and conclusions.

2. Pocket resonances and barrier resonances

In [3] we described the nature of resonances using an exactly solvable repulsive Eckart potential for the s-wave without any pocket. The resulting formula for the resonance energy and width was found to be suitable for $^{12}C + {}^{12}C$ and $^{12}C + {}^{16}O$ systems. To elucidate additional features of barrier states, we make a comparative study of the potential pocket resonances and barrier resonances using both rectangular and Woods–Saxon shape barriers and also elucidate the role of absorption in the pocket region in both the cases.

2.1. Rectangular potential barrier

Let us consider the s-wave resonances generated by the potential $U(r) = \hbar^2 V(r)/2\mu$ where $V(r)$ is in units of fm^{-2} and

$$\begin{aligned} V(r) &= 0 \qquad r \leqslant a \quad r \geqslant b \quad b > a \\ &= V_0 \qquad a < r < b. \end{aligned} \tag{8}$$

This is an idealized example of a potential having a pocket ($r \leqslant a$) and a barrier ($a < r < b$) region. One can expect that in the pocket region in the case of an s-wave the potential will generate very long-lived states which are close to the corresponding levels of the one-dimensional box of range a. The lifetime of these states will be

governed by the penetrability factor from the pocket to the outside region ($r \geq b$). On the other hand, since the system will have reduced kinetic energy in the barrier, one may expect generation of FRBRS also, dominated by the region $a < r < b$. Their width will be substantially larger than the width of the PRS since these states do not have to penetrate a barrier for decay. Also, we can expect that wavefunctions associated with the FRBRS should be dominant in the barrier region.

Solving the s-wave Schrödinger equation

$$\frac{d^2\Psi}{dr^2} + [k^2 - V(r)]\Psi = 0 \tag{9}$$

where $k^2 = 2mE/\hbar^2$, for the potential given by (8) we get the following expression for the s-wave S-matrix:

$$S(k) = e^{-2ikb}\left[\frac{(1+\alpha/k)A\, e^{i\alpha b} + (1-\alpha/k)B\, e^{-i\alpha b}}{(1-\alpha/k)A\, e^{i\alpha b} + (1+\alpha/k)B\, e^{-i\alpha b}}\right] \tag{10}$$

where

$$A = [\sin ka - (ik/\alpha)\cos ka]\, e^{-i\alpha a}/2 \tag{11}$$

$$B = [\sin ka + (ik/\alpha)\cos ka]\, e^{i\alpha a}/2 \tag{12}$$

$$\alpha = (k^2 - V_0)^{1/2}. \tag{13}$$

The resonance poles of this S-matrix can be obtained by searching for the zeros of the denominator in (10), in the lower half of the complex k plane. Based on a numerical search for such zeros, a number of poles or resonance positions of $S(k)$ in the complex k and complex k^2 planes are obtained. The results are listed in table 1.

We find that potential pocket resonances with energy $\mathrm{Re}\, k_R^2 < V_0$ are extremely narrow (small $\mathrm{Im}\, k_R^2$). Their imaginary parts are related to the decay constant

$$\lambda \simeq \frac{2\hbar}{R\mu}\left[\frac{V_0 + k^2}{(V_0 - k^2)^{1/2}}\right] \exp\left[-2\int_a^b (V_0 - k^2)^{1/2}\, dr\right]. \tag{14}$$

This relation explains the extremely small imaginary part of the resonance poles for the PRS listed in table 1. In contrast, the imaginary part of the FRBRS are much larger. The sharpest FRBR is closest to the barrier; the other two are somewhat distant from the barrier top (see table. 1). We have also carried out the numerical search for resonance poles for the barrier $V(r) = V_0$, $r \leq a$; $V(r) = 0$, $r > a$ and did not find any resonance pole having an energy less than V_0. This can perhaps be attributed to a

Table 1. Pocket and barrier resonance positions in the complex k plane in the case of a shifted rectangular repulsive barrier, see (8), with parameters $V_0 = 10.0\ \mathrm{fm}^{-2}$, $a = 3.0$ fm and $b = 6.0$ fm.

Nature of poles	Resonance pole	k (fm^{-1})	k^2 (fm^{-2})
Pocket poles	I	$0.94 - 0.13 \times 10^{-8}$i	$0.89 - 0.2 \times 10^{-8}$i
	II	$1.88 - 0.60 \times 10^{-6}$i	$3.54 - 0.2 \times 10^{-6}$i
	III	$2.78 - 0.23 \times 10^{-3}$i	$7.74 - 0.1 \times 10^{-3}$i
Barrier poles	IV	3.31 − 0.026i	10.96 − 0.173i
	V	3.89 − 0.087i	15.16 − 0.677i
	VI	4.36 − 0.125i	19.04 − 1.093i

large reflection from the sharp edge at $r = a$ and a small transmission on to the barrier region for $E < V_0$.

One way to visualize the distinction between PRS and FRBRS is to determine the localization of the corresponding wavefunctions in the coordinate space. In figure 1 we have shown the variation of the modified s-wave radial wavefunction $\Psi(r)$ ($\Psi(r) \simeq \sin kr$ as $r \to 0$) in the region of the pocket and the barrier at resonance energies (real part of the pole positions in the complex k^2 plane) both above and below the barrier height. It is clear that PRS are characterized by a typical bound-state-like behaviour inside the pocket and damp out in the barrier region (see figures 1(a–c)). Of course it will pick up sinusoidal oscillations outside the barrier ($r \geq b$) since the resonance energy is positive. On the other hand the wavefunctions corresponding to the FRBRS (figures 1(d–f)) are characterized by enhanced oscillations in the barrier region, and comparatively less amplitude in the pocket region. However, in the case of resonances further above the barrier the amplitude of the wavefunction $|\Psi|$ is comparable both in the pocket and barrier regions, but still the predominance in the barrier region is retained. This indicates that the barrier is less important in the case of PRS but dominates the barrier region states.

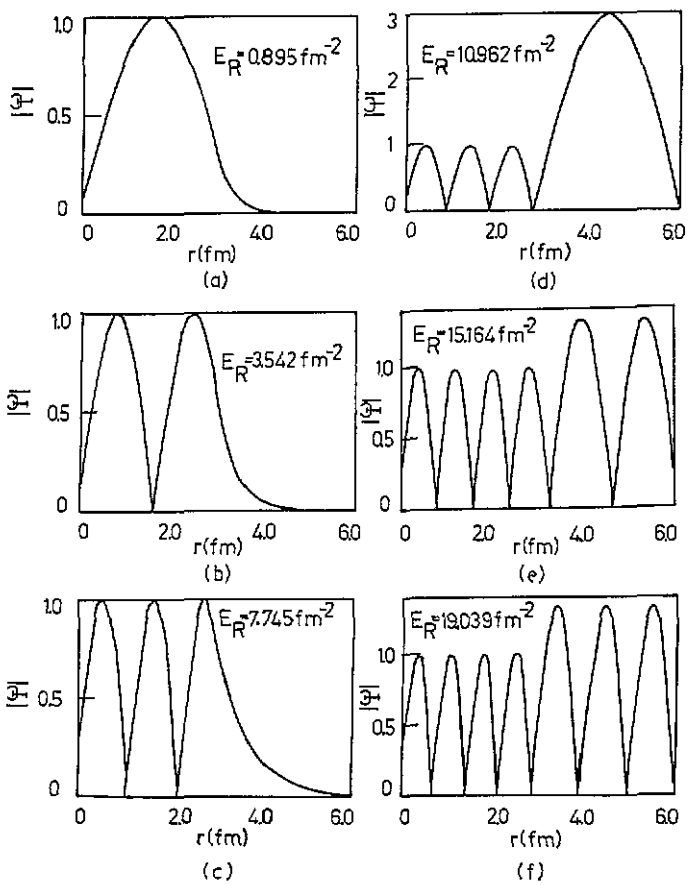

Figure 1. The variation of the modified s-wave radial wavefunction $|\Psi|$ against r corresponding to (a–c) pocket and (d–f) barrier resonances of a potential given by (8). The amplitudes of the wavefunctions are normalized to one at their first maximum. Here $V_0 = 10.0\ \text{fm}^{-2}$, $a = 3.0$ fm and $b = 6.0$ fm.

The situation when the pocket is absorptive can be studied using the potential

$$\begin{aligned} V(r) &= iW \qquad r \leqslant a \quad W < 0 \\ &= V_0 \qquad a < r < b \\ &= 0 \qquad r \geqslant b \end{aligned} \tag{15}$$

where V_0 is a positive quantity. This is an idealized example of an absorptive pocket and transparent barrier. In table 2 we list the variation of typical PR and FRBR positions with W. It is seen that $\mathrm{Im}\, k_R^2$ in the case of PRS is very close to the imaginary part W of the potential $V(r)$. This illustrates that the widths of the PRS will be approximately W whereas the widths of the resonances associated with the non-absorptive barrier are affected to a lesser extent (but not negligible) by the absorptive pocket.

2.2. *Barrier with Woods–Saxon shape with an absorptive pocket*

The discussion in the last section using a rectangular barrier and pocket can be made more realistic by using a smoother barrier with an absorptive pocket. Such an analysis is important in correlating the nature of barrier region resonances as specified in [5] and the nature of resonances with an ordinary repulsive potential barrier. The barrier region resonances studied in [5] obtained using a repulsive potential barrier were uninfluenced by reflection at $r = 0$. This was accomplished by either allowing r to extend to $-\infty$, or by putting adequate absorption inside the region. In this section we compare the results for barrier states with (i) the boundary condition $\Psi = 0$ at the interior edge of the barrier and (ii) with a barrier having a highly absorptive pocket for its interior, to clarify the differences between the two approaches.

For the model calculations we used the potential

$$V(r) = V_R(r) + iV_I(r) \tag{16}$$

where

$$\begin{aligned} V_R(r) &= V_0/\{1 + \exp[(R_0 - r - C_1)/a_1]\} \qquad r \leqslant R_0 \\ &= V_0/\{1 + \exp[(r - R_0 - C_2)/a_2]\} \qquad r > R_0 \end{aligned} \tag{17}$$

$$V_I(r) = W_0/\{1 + \exp[(r - R_0 + C_W)/a_W]\} \qquad W_0 < 0. \tag{18}$$

Figure 2 indicates the shape of the potential for a typical set of parameters. The ratios C_1/a_1 and C_2/a_2 are chosen large enough compared to unity such that the barrier is reasonably flat and $V_R(r)$ has continuity at $r = R_0$ for all practical computation purposes. Absorption in the pocket region can be varied by varying W_0. In figure 3 we indicate the location of three pocket region poles and two barrier region poles in the complex k^2 plane obtained using this potential for different

Table 2. Illustration of the variation of pocket and barrier pole positions for different strengths of the imaginary part (W) of the potential given by (15) (see text) with parameters $V_0 = 10.0\ \mathrm{fm}^{-2}$, $a = 3.0$ fm and $b = 6.0$ fm.

	Typical PR poles, k^2 (fm^{-2})		Typical barrier resonance poles, k^2 (fm^{-2})	
$\lvert W\rvert$ (fm^{-2})	(i)	(ii)	(i)	(ii)
0.0	$0.894 - 0.25 \times 10^{-8}$i	$3.541 - 0.3 \times 10^{-6}$i	10.962 − 0.173i	15.164 − 0.677i
0.4	0.894 − 0.396i	3.542 − 0.383i	10.952 − 0.209i	15.171 − 0.829i
1.2	0.895 − 1.189i	3.546 − 1.151i	10.940 − 0.276i	15.147 − 1.138i
2.0	0.897 − 1.982i	3.550 − 1.920i	10.936 − 0.327i	15.071 − 1.459i

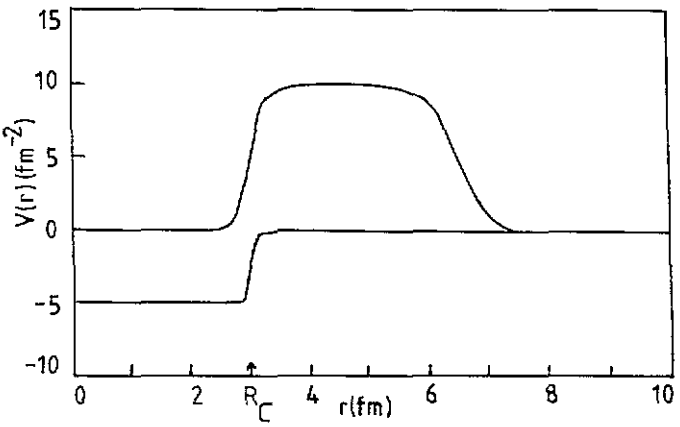

Figure 2. Plot of the potential having a barrier with a Woods–Saxon shape with an absorptive pocket, for a typical set of parameters. The parameters used are $V_0 = 10\ \text{fm}^{-2}$, $W_0 = -5\ \text{fm}^{-2}$, $R_0 = 4.5$ fm, $C_1 = 1.5$ fm, $C_2 = 2.0$ fm, $C_w = 1.5$ fm, $a_1 = 0.12$ fm, $a_2 = 0.25$ fm and $a_w = 0.05$ fm.

strengths of absorption. The use of the complex k^2 plane rather than the complex k plane is preferred because the real and imaginary parts of the resonance poles in the k^2 plane are directly related to resonance energies and widths. It may be noted that the real parts of the pole positions for both pocket and barrier resonances do not vary much when absorption is increased. However, as expected it is seen that $\text{Im}\, k_R^2$ in the case of PR is very close to the strength W_0 of the $V_I(r)$. But in the case of barrier resonance closest to the threshold the variation of $\text{Im}\, k_R^2$ with respect to W_0 is relatively small compared to the corresponding PR. This indicates that the barrier with an absorptive pocket does not affect the position of the FRBR.

Now we examine the correlation between the barrier region resonances generated in the presence of an absorptive pocket on the interior side of the pocket (case A) and the resonances generated by an ordinary potential barrier. In order to eliminate the absorptive pocket in potential (16) we introduce a hard core at $r = R_c$

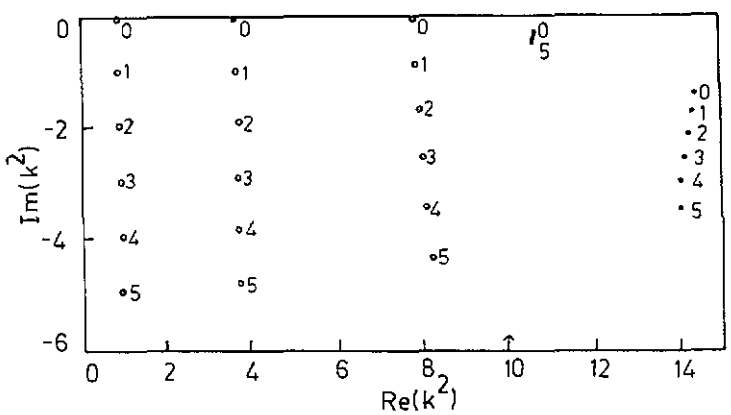

Figure 3. The location of pocket and barrier region resonance poles in the complex k^2 plane in units of fm^{-2} obtained using the potential given by (16) for different strengths (W_0) of absorption. The other parameters are as in figure 2. The open circles represent pocket resonance poles and the solid circles represent barrier region resonance poles. The numbers next to the pole positions indicate $-W_0$ in units of fm^{-2}. The arrowhead indicates the barrier top.

Table 3. Barrier region resonance positions in the complex k plane in the case of a potential given by (16) having a barrier with a Woods–Saxon shape and a highly absorptive pocket with $W_0 = -20\,\mathrm{fm}^{-2}$ (case A) and a potential given by (16) but with a hard core at $r = R_c = 3.0\,\mathrm{fm}$ (case B). The other potential parameters are listed in the caption of figure 2.

Barrier resonance poles	Case A, k (fm^{-1})	Case B, k (fm^{-1})
I	3.263 − 0.06801i	3.281 − 0.05872i
II	3.984 − 0.4607i	4.096 − 0.3702i
III	4.502 − 0.7018i	4.410 − 0.5670i

such that $\Psi(r) = 0$ at $r \leqslant R_c$ and analyse the nature of resonance poles generated. R_c is close to the interior edge of the barrier (figure 2). We refer to this as case B. This is akin to the model for barrier region resonances used in [3]. In table 3 we list the barrier region resonances, in the complex k plane obtained by potentials corresponding to case A and case B. The comparison of pole positions indicate that the barrier resonance poles in both case A and case B are not very different.

The physical reason for this can be analysed by comparing the modified s-wave radial wavefunctions corresponding to case A with a high absorption ($W_0 = -20\,\mathrm{fm}^{-2}$) and case B at energy k^2 close to the barrier. In figure 4 we indicate $|\Psi|$ at $k^2 = 10.74\,\mathrm{fm}^{-2}$ corresponding to both case A and case B, respectively, normalized such that both have the same highest peak. This illustrates that introducing a high absorption at $r < R_c$ gives approximately the same wavefunction in the barrier region and outside as that of an ordinary barrier with an infinite repulsion at $r = R_c$. It is clear that if $|W_0|$ is made still larger the damping of $|\Psi|$ in the absorptive pocket will be much more rapid. Thus, the barrier with a strong absorptive pocket gives rise to a wavefunction which is quite similar to the wavefunction of a repulsive barrier with infinite repulsion ($\Psi = 0$) at the interior edge of the barrier.

Since heavy-ion scattering is dominated by the barrier region and the interior region is highly absorptive, and the potential is much better known in the barrier

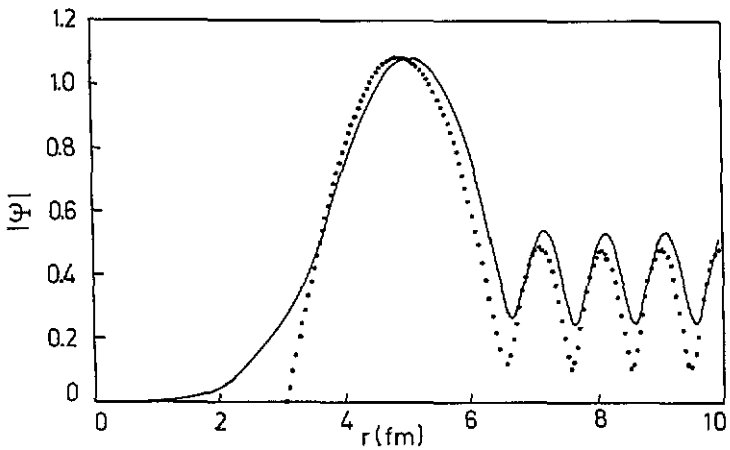

Figure 4. The modified s-wave radial functions near a barrier region resonance pole. The full line corresponds to case A and the dotted line corresponds to case B (see text). Here $k^2 = 10.74\,fm^{-2}$ and $W_0 = -20\,\mathrm{fm}^{-2}$. All other parameters are as in figure 2.

region than in the nuclear well region, the dominant mechanism of many heavy-ion resonances can be expected to be barrier region resonances. Moreover, the strong enhancement of the wavefunction in the vicinity of the barrier suggests that the nuclei orbit in the resonance states with a relative distance given by the barrier position. The model calculations discussed in this section indicate that the positions of resonance poles above the barrier are only marginally affected when we replace the absorptive pocket by a hard core at the interior edge of the barrier. There is a close similarity in the behaviour of $|\Psi|$ in the barrier region. The present approach provides a good scheme to study to what extent heavy-ion resonances can be attributed to barrier region resonances. This is clear in view of the fact that the effective potential, including the centrifugal term, for most of the relevent partial waves is dominated by the barrier region, and the corresponding wavefunction to the left of the barrier becomes highly damped due to the combined effect of high absorption and a large centrifugal barrier.

3. Barrier region resonance model for the $^{16}O + ^{16}O$ system

3.1. Resonances generated by a truncated parabolic barrier

The analytical formula used in the analysis of $^{12}C + ^{12}C$ and $^{12}C + ^{16}O$ systems [3] was based on the S-matrix for the repulsive Eckart potential which gave $(n + \frac{3}{4})^2$ dependence on the resonance energies. However, an examination of available experimental data [6–8] in the $^{16}O + ^{16}O$ system indicates that resonance energies for a given partial wave are approximately equispaced. The immediate idea one then has is to interpret them in terms of a suitably structured rotation–vibration model with the approximate equispaced resonances being generated by a parabolic barrier. The approaches of [8] are motivated by potentials which generate resonance states in the potential pocket region. However, we note that in the vicinity of the barrier one can have resonance states generated by the barrier itself. In this paper we restrict ourselves to interpreting the heavy-ion resonances within the framework of barrier region resonances.

In view of the approximately equispaced resonance energies for a given l in the $^{16}O + ^{16}O$ system we investigate whether an inverted finite-range parabolic barrier can generate in the vicinity of the barrier approximately equispaced resonances. In order to do this we studied the s-wave S-matrix numerically, for the finite-range inverted parabolic barrier given by

$$\begin{aligned} V(r) &= V_0 - \beta r^2/2 \qquad r < R \\ &= 0 \qquad\qquad\quad r \geqslant R \end{aligned} \tag{19}$$

where

$$R = (2V_0/\beta)^{1/2}.$$

This potential is of interest because in the case of the infinite-range harmonic oscillator barrier, BTR poles in the complex energy plane for different partial waves l were given by (7), indicating that the number of resonances of increasing width are situated at resonance energies close to the barrier top. Hence the corresponding result in the case of a finite-range truncated parabolic barrier is of more interest in the context of potential scattering. In table 4 we list several pole positions of the s-wave S-matrix in the complex k^2 plane in the case of a potential given by (19) for different values of β. It is interesting to note that there are resonances both below

and above the barrier and their spacings and widths indicate some approximate symmetry. It is also interesting to note that the two levels in the immediate vicinity of the barrier are approximately equispaced with respect to the resonance closest to the barrier. This linearity is gradually destroyed in the case of levels further away both above and below the barrier.

We know that in the case of a harmonic well $-U_0 + m\omega^2 r^2/2$ of depth U_0 the s-wave energy levels are given by the formula

$$E_n = -U_0 + (2n + \tfrac{3}{2})\hbar\omega \tag{20}$$

indicating a spacing of $2\hbar\omega$ between the adjacent levels. In this case the ground state energy is $3/2\hbar\omega$ above the bottom of the well. On the other hand the corresponding barrier resonances occur very close to the barrier top. But in our analysis using a large amount of data we found that the spacing between the barrier top level and the next adjacent level on the either side is approximately in the range $(2)^{1/2}$ to $2\hbar\omega$. However, due to the finite-range harmonic barrier and the fact that resonant states do not decay exponentially, anharmonic terms significantly affect the levels away from barrier top. The nonlinearity or unharmonicity becomes important even for $n = 2$ (assuming the level closest to the barrier top to be $n = 0$), as is clear from table 4. We also observe that the sharpest resonance is practically on the top of the barrier.

Another interesting aspect which we noted is that $\mathrm{Im}\, k_R^2$ of two levels adjacent to the barrier top are approximately the same, indicating resonances of the same width. In order to interpret this we calculated the transit time for a classical particle to slide down the truncated harmonic oscillator barrier in the classically allowed region for energy $E_\pm = U_0 \pm \Delta$, $\Delta < U_0$. We find that these two items are given by the same formula,

$$\tau_\pm = (m/2)^{1/2} U_0^{-1/2} R \ln\left[\frac{U_0^{1/2} + E^{1/2}}{[\pm(E - U_0)]^{1/2}}\right]. \tag{21}$$

Further, it may be noted that for a given R, τ is proportional to $U_0^{-1/2}$, indicating that for FRBRS the width will increase with barrier height, for a given range R. Similar results are obtained in the case of the repulsive Eckart potential [3].

The calculations on the repulsive Eckart potential [3], the square well barrier, the barrier with a Woods–Saxon shape and the finite-range harmonic barrier indicate that different resonance level spacings can be expected if one uses different types of

Table 4. Resonance positions in the complex k^2 plane in the case of cut-off parabolic barrier represented by (19).

k^2 (fm^{-2})		
$\beta = 0.1$ fm^{-4} $V_0 = 10$ fm^{-2}	$\beta = 0.2$ fm^{-4} $V_0 = 10$ fm^{-2}	$\beta = 0.3$ fm^{-4} $V_0 = 10$ fm^{-2}
11.30 − 0.6953i	12.14 − 1.1074i	12.67 − 1.389i
10.56 − 0.5597i	10.94 − 0.8407i	11.11 − 1.051i
10.01 − 0.4472i	10.06 − 0.6299i	10.01 − 0.7762i
9.448 − 0.5524i	9.224 − 0.7794i	8.891 − 1.008i
8.673 − 0.6700i	7.994 − 0.9923i	7.186 − 1.306i

potential barrier. This can be fruitfully exploited in constructing the appropriate models for the description of heavy-ion resonances

3.2. Analysis of the data

Based on the above discussion on the truncated inverted harmonic oscillator barrier and noting that in the case of the $^{16}O + ^{16}O$ system the number of observed resonance states in the Coulomb barrier region is less than or equal to five, we seek to analyse these resonances using the empirical expression

$$E(n,l) = V_B^{(l)} + (C_0 + C_1 l^2)n + \varepsilon n^2 \qquad n = 0, \pm 1, \pm 2 \tag{22}$$

where $V_B^{(l)}$ is the height of the barrier for the lth partial wave, and C_0, C_1 and ε are parameters. The heights of the effective potential $V_B^{(l)}$ for different ls have been calculated using the global nucleus–nucleus potential [9]

$$V(r) = -50(R_1R_2)/(R_1 + R_2)\exp[(R_1 + R_2 - r)/a] \tag{23}$$

where

$$R_i = 1.233A_i^{1/3} - 0.978A_i^{-1/3}\text{fm} \qquad (i = 1, 2)$$

$$a = 0.63\text{fm}$$

along with centrifugal and Coulomb potentials. $C_1 l^2$ is the term which takes into account the fact that the effective barrier varies slowly with l. ε accounts for the deviation from the linear dependence of n in the neighbourhood of the barrier. This expression is based on the assumption that in the vicinity of the barrier the effective potential has a height $V_B^{(l)}$ and a shape close to an inverted harmonic oscillator. In such a situation a reasonable parametrization for the barrier resonances is given by (22). In this parametrization $V_B^{(l)}$ incorporates the $l(l+1)/r^2$ term, implying that the present model is also akin to the rotation–vibration model, even though the term 'rotation–vibration state' may not be appropriate in our model since our description is based on the model of orbiting states around the barrier.

Table 5. The quantities $R_B^{(l)}$, $V_B^{(l)}$ and a typical set of $E(n,l)$ corresponding to the $^{16}O + ^{16}O$ system. The parameters used to compute $E(n,l)$ are $C_0 = 0.7478$ MeV, $C_1 = 0.00127$ MeV and $\varepsilon = 0.1724$ MeV.

			$E(n,l) = V_B^{(l)} + (C_0 + C_1 l^2)n + \varepsilon n^2$ (MeV)				
l	$R_B^{(l)}$ (fm)	$V_B^{(l)}$ (MeV)	$n = -2$	-1	0	1	2
2	8.09	10.70	9.89	10.12	10.70	11.63	12.90
4	8.03	11.27	10.43	10.68	11.27	12.21	13.51
6	7.93	12.18	11.28	11.55	12.18	13.15	14.46
8	7.81	13.44	12.47	12.79	13.44	14.45	15.80
10	7.67	15.10	14.04	14.40	15.10	16.15	17.55
12	7.54	17.18	16.00	16.42	17.18	18.29	19.74
14	7.40	19.71	18.40	18.88	19.71	20.89	22.41
16	7.27	22.73	21.26	21.82	22.73	23.98	25.57
18	7.13	26.26	24.62	25.27	26.26	27.61	29.29
22	6.88	35.02	32.96	33.82	35.02	36.57	38.47
24	6.76	40.31	38.01	38.99	40.31	41.99	44.00

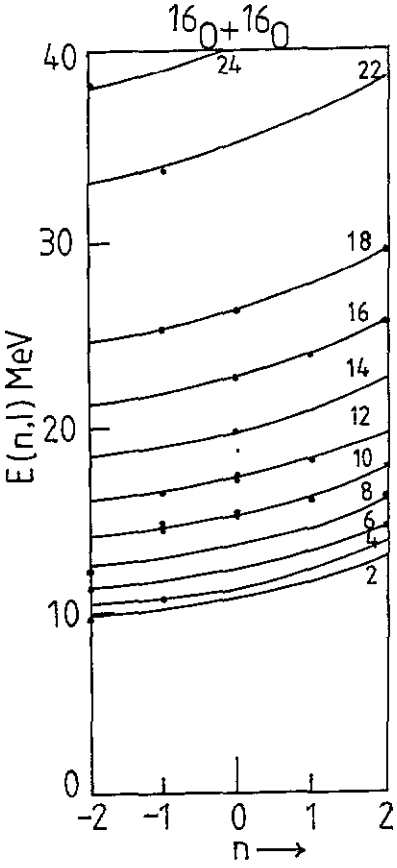

Figure 5. Plots of $E(n,l)$ against the assumed values of n for the resonance data of the $^{16}O + ^{16}O$ system. The parameters used are listed in table 5. The experimental data (solid circles) are from [6–8].

The barrier resonance states occur somewhat symmetrically around the barrier in the case of a truncated parabolic barrier. Hence, it is natural to designate the states above and below the barrier using n taking values $0, \pm 1, \pm 2$, etc. The quantities n and l together determine the energy of the resonance states.

Using this formula we have fitted the experimental data for the $^{16}O + ^{16}O$ system. The experimental data closest to the barrier top $E(n,l) \approx V_B^{(l)}$ correspond to the $n = 0$ level, and those above and below are assigned positive and negative values, respectively. The resonance energies obtained using (22) are listed in table 5. In figure 5 we depict the results obtained for even l alone with experimental data. It is clear that the present approach gives quite a good fit to the experimental data. This fit to the experimental data also implies that in this parametrization, the relation between the energy levels and the $l(l+1)$ term incorporating the rotational aspects of motion is also automatically taken care of.

4. Discussion and conclusions

We will now summarize the main results of the present paper, and follow this by some discussions on resonances in heavy-ion scattering. We have analysed two

categories of resonances which can be identified in scattering from a finite-range potential with a pocket followed by a barrier. If the potential is real, PRS will be more important because of their narrower widths. However, if the pocket is highly absorptive, the scattering will be dominated by resonance states dominant in the barrier region.

It should be mentioned that within the framework of the WKB approximation, Brink [9] also studied resonances generated by the barrier region. The FRBR states are somewhat different from the BTRS defined in terms of an infinite-range parabolic barrier given in [5]. In particular, FRBRS have different energies, unlike the BTRS in [5]. Grama *et al* in their recent paper [4] present a global method to identify all the S-matrix poles in the k-plane for a central potential. They came to the conclusion that a potential with a complex well followed by a real barrier can support two types of resonance poles (those localized in the potential well and those localized outside the potential well), which is consistent with our definition of PRS and FRBRS. Their work also supports our model [3] for heavy-ion resonances.

The present approach for the analysis of heavy-ion resonance data comes within the general framework of potential scattering, that is if the potential pocket is highly absorptive resonances can be attributed to the barrier region. It may be noted that in the case of the $^{16}O + {}^{16}O$ system, studies of resonance have been carried out using different approaches such as the orbiting cluster model [10] and using shallow potentials [11–14], deep potentials [15, 16] and potentials such as the Morse and anharmonic well [8, 17]. The orbiting cluster model essentially incorporates implicitly the spirit of barrier region resonances in the sense that resonances for a given l are in effect rotating clusters with a separation approximately corresponding to the barrier. The calculations based on the effective shallow potential is somewhat akin to the present approach.

The deep potential approach [15, 16] is quite interesting. This potential also gives a barrier position approximately equal to that obtained by using a global nucleus–nucleus potential. However, it gives a deeper pocket because of the large values of the strength of the attractive part of the nuclear potential. In [16] the strength of the imaginary part in the pocket is 2.5 MeV. In the absence of an imaginary part such a deep potential can be expected to generate very sharp resonances but their widths will be drastically enhanced and will be of the order of W if the imaginary part is present. Even in such potentials if the barrier region is surface transparent, one can expect resonances close to the barrier to be narrower because the imaginary part of the potential will affect them to a comparatively lesser extent. This point is illustrated using model calculations in section 2. These demonstrate the fact that in the case of a surface transparent potential (a small imaginary part in the barrier region and a large imaginary part in the pocket region) the FRBRS are more important than the PRS.

In the case of the $^{16}O + {}^{16}O$ system the spacing between the levels is of the order of 0.6 to $\approx$1 MeV [6], and hence one expects their widths to be in the kiloelectronvolt region. Hence, even in the fits obtained using the deep potential the resonances are perhaps dominated only by the barrier.

In the case of long-range (16 fm) potentials used in [8, 17], the minima of the effective potential are almost at the Coulomb barrier position. Hence, by construction, the potentials used are such that they generate PR states in the vicinity of the barrier. Such long-range potentials may have to be interpreted in terms of extremely

deformed shapes of the colliding systems, whereas our model can be visualized in terms of the usual heavy-ion collisions dominated by the barrier region.

The approach in the present and earlier paper [3] essentially emphasizes the point that in potential scattering, resonances can be classified broadly in two categories namely pocket and barrier resonances, and in the description of heavy-ion resonances the barrier resonance is more appropriate since the pocket region is highly absorptive. It may also be noted that in [3] FRBRS has been applied to the $^{12}C + ^{12}C$ and $^{12}C + ^{16}O$ systems using the model based on the resonances generated by the repulsive Eckart potential. Thus the results of [3] and the present paper complete the analysis of heavy-ion resonances in three important cases within the framework of the barrier region resonance model.

Acknowledgments

We thank Professor R Singh and Professor Y K Gambhir for useful discussions.

References

[1] D. Alfaro V and Regge T 1965 *Potential Scattering* (Amsterdam: North-Holland)
[2] Newton R G 1966 *Scattering Theory of Waves and Particles* 2nd edn (New York: McGraw Hill) p 357
[3] Sahu B, Jyrwa B M, Susan P and Shastry C S 1991 *Phys. Rev.* C **44** 2729
[4] Cornelia Grama, Grama N and Zamfirescu I 1992 *Ann. Phys., NY* **218** 346
[5] Friedman W A and Goebel C J 1977 *Ann. Phys., NY* **104** 145
[6] Cindro N 1981 *Riv. Nuovo Cimento* **4** 1
[7] Cindro N 1988 *Ann. Phys., Paris* **13** 289
[8] Abbondanno U, Datta S, Cindro N, Basarak Z and Vannine G 1989 *J. Phys. G: Nucl. Phys.* **15** 1845
[9] Brink D M 1985 *Semiclassical Methods for Nucleus-Nucleon Scattering* (Cambridge: Cambridge University Press) p 105
[10] Cindro N and Bozin M 1989 *Ann. Phys., Paris* **192** 307
[11] Maher J V, Sachs M W, Siemssen R H, Weidinger A and Bromley D A 1969 *Phys. Rev.* **188** 1665
[12] Chatwin R A, Eck J S, Robson D and Ritcher A 1970 *Phys. Rev.* C **1** 795
[13] Gobbi A, Weiland R, Chua L, Shapira D and Bromley D A 1973 *Phys. Rev.* C **7** 30
[14] Pantis G, Ionannidis K and Poirer P 1985 *Phys. Rev.* C **32** 657
[15] Kondo Y, Robson B A and Smith R 1989 *J. Phys. Soc. Japan* **58** 597
[16] Kondo Y, Robson B A and Smith R 1989 *Phys. Lett.* **227B** 310
[17] Sathpathy L, Pradip K Sahu and Sarangi P 1992 *J. Phys. G: Nucl. Part. Phys.* **18** 1793